NASA/TM—2015-218892

A Fully Nonmetallic Gas Turbine Engine Enabled by Additive Manufacturing

Part III: Additive Manufacturing and Characterization of Ceramic Composites

Michael C. Halbig and Joseph E. Grady
Glenn Research Center, Cleveland, Ohio

Mrityunjay Singh
Ohio Aerospace Institute, Brook Park, Ohio

Jack Ramsey, Clark Patterson, and Tom Santelle
Rapid Prototyping+Manufacturing (rp+m), Avon Lake, Ohio

December 2015

NASA STI Program . . . in Profile

Since its founding, NASA has been dedicated to the advancement of aeronautics and space science. The NASA Scientific and Technical Information (STI) Program plays a key part in helping NASA maintain this important role.

The NASA STI Program operates under the auspices of the Agency Chief Information Officer. It collects, organizes, provides for archiving, and disseminates NASA's STI. The NASA STI Program provides access to the NASA Technical Report Server—Registered (NTRS Reg) and NASA Technical Report Server—Public (NTRS) thus providing one of the largest collections of aeronautical and space science STI in the world. Results are published in both non-NASA channels and by NASA in the NASA STI Report Series, which includes the following report types:

- TECHNICAL PUBLICATION. Reports of completed research or a major significant phase of research that present the results of NASA programs and include extensive data or theoretical analysis. Includes compilations of significant scientific and technical data and information deemed to be of continuing reference value. NASA counter-part of peer-reviewed formal professional papers, but has less stringent limitations on manuscript length and extent of graphic presentations.

- TECHNICAL MEMORANDUM. Scientific and technical findings that are preliminary or of specialized interest, e.g., "quick-release" reports, working papers, and bibliographies that contain minimal annotation. Does not contain extensive analysis.

- CONTRACTOR REPORT. Scientific and technical findings by NASA-sponsored contractors and grantees.

- CONFERENCE PUBLICATION. Collected papers from scientific and technical conferences, symposia, seminars, or other meetings sponsored or co-sponsored by NASA.

- SPECIAL PUBLICATION. Scientific, technical, or historical information from NASA programs, projects, and missions, often concerned with subjects having substantial public interest.

- TECHNICAL TRANSLATION. English-language translations of foreign scientific and technical material pertinent to NASA's mission.

For more information about the NASA STI program, see the following:

- Access the NASA STI program home page at http://www.sti.nasa.gov

- E-mail your question to help@sti.nasa.gov

- Fax your question to the NASA STI Information Desk at 757-864-6500

- Telephone the NASA STI Information Desk at 757-864-9658

- Write to:
  NASA STI Program
  Mail Stop 148
  NASA Langley Research Center
  Hampton, VA 23681-2199

NASA/TM—2015-218892

A Fully Nonmetallic Gas Turbine Engine Enabled by Additive Manufacturing

Part III: Additive Manufacturing and Characterization of Ceramic Composites

Michael C. Halbig and Joseph E. Grady
Glenn Research Center, Cleveland, Ohio

Mrityunjay Singh
Ohio Aerospace Institute, Brook Park, Ohio

Jack Ramsey, Clark Patterson, and Tom Santelle
Rapid Prototyping+Manufacturing (rp+m), Avon Lake, Ohio

National Aeronautics and
Space Administration

Glenn Research Center
Cleveland, Ohio 44135

December 2015

Acknowledgments

The authors would like to thank Drs. Mike Dudley and Koushik Datta from NASA Aeronautics Research Institute for their continuous support and encouragement. The authors would also like to thank Ron Phillips (Vantage Partners, LLC) for mechanical testing, Joy Buehler (Vantage Partners, LLC) for epoxy mounting and polishing of samples, and Gerald Hurd (NASA GRC) for conducting 1450 °C heat treatment furnace runs. This work was supported by the NASA Aeronautics Research Institute (NARI) Program.

Level of Review: This material has been technically reviewed by technical management.

Available from

NASA STI Program
Mail Stop 148
NASA Langley Research Center
Hampton, VA 23681-2199

National Technical Information Service
5285 Port Royal Road
Springfield, VA 22161
703-605-6000

This report is available in electronic form at http://www.sti.nasa.gov/ and http://ntrs.nasa.gov/

A Fully Nonmetallic Gas Turbine Engine Enabled by Additive Manufacturing
Part III: Additive Manufacturing and Characterization of Ceramic Composites

Michael C. Halbig and Joseph E. Grady
National Aeronautics and Space Administration
Glenn Research Center
Cleveland, Ohio 44135

Mrityunjay Singh
Ohio Aerospace Institute
Brook Park, Ohio 44142

Jack Ramsey, Clark Patterson, and Tom Santelle
Rapid Prototyping+Manufacturing (rp+m)
Avon Lake, Ohio 44012

Abstract

This publication is the third part of a three part report of the project entitled "A Fully Nonmetallic Gas Turbine Engine Enabled by Additive Manufacturing" funded by NASA Aeronautics Research Institute (NARI). The objective of this project was to conduct additive manufacturing to produce ceramic matrix composite materials and aircraft engine components by the binder jet process. Different SiC powders with median sizes ranging from 9.3 to 53.0 μm were investigated solely and in powder blends in order to maximize powder packing. Various infiltration approaches were investigated to include polycarbosilane (SMP-10), phenolic, and liquid silicon. Single infiltrations of SMP-10 and phenolic only slightly filled in the interior. When the SMP-10 was loaded with sub-micron sized SiC powders, the infiltrant gave a much better result of filling in the interior. Silicon carbide fibers were added to the powder bed to make ceramic matrix composite materials. Microscopy showed that the fibers were well distributed with no preferred orientation on the horizontal plane and fibers in the vertical plane were at angles as much as 45°. Secondary infiltration steps were necessary to further densify the material. Two to three extra infiltration steps of SMP-10 increased the density by 0.20 to 0.55 g/cc. However, the highest densities achieved were 2.10 to 2.15 g/cc. Mechanical tests consisting of 4 point bend tests were conducted. Samples from the two CMC panels had higher strengths and strains to failure than the samples from the two nonfiber reinforced panels. The highest strengths were from Set N with 65 vol% fiber loading which had an average strength of 66 MPa. Analysis of the fracture surfaces did not reveal pullout of the reinforcing fibers. Blunt fiber failure suggested that there was not composite behavior. The binder jet additive manufacturing method was used to also demonstrate the fabrication of turbine engine vane components of two different designs and sizes. The binder jet method has benefits over the conventional manufacturing of CMCs in that prototype and production parts can be fabricated quickly and economically with no tooling and extensive hand layup.

Introduction

Ceramic matrix composites (CMCs) with their continuous fiber reinforcement, high fracture toughness, and favorable strengths are very promising materials for high temperature structural applications. The elevated temperature capability and lower cooling requirements of CMCs make them particularly beneficial for replacing metallic components in turbine engine applications. These capabilities allow for improved fuel efficiency and reduced emissions. Silicon carbide fiber reinforced silicon carbide

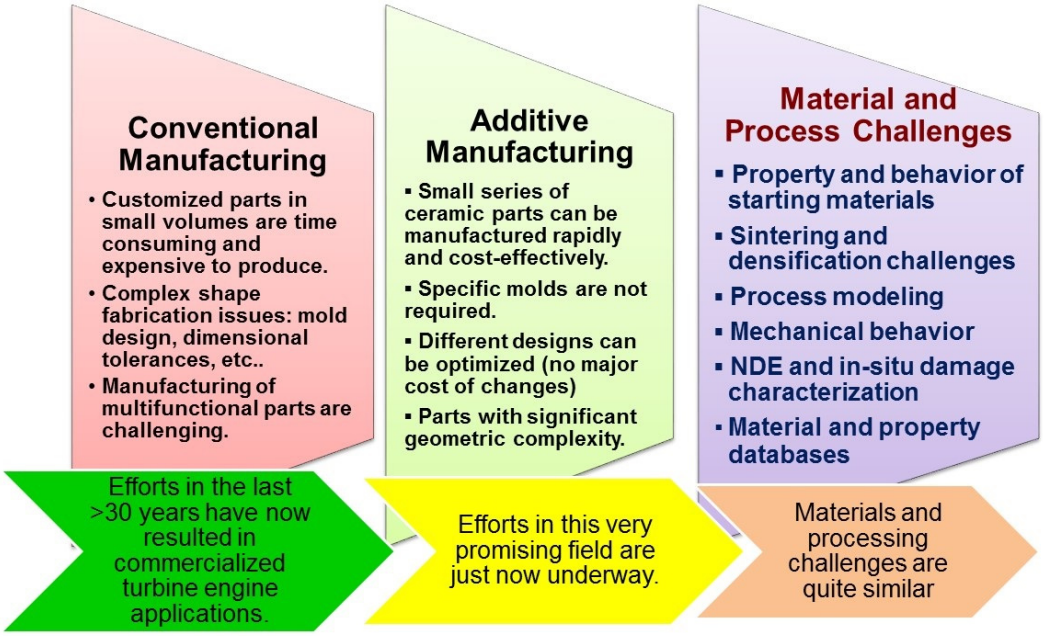

Figure 1.—Conventional manufacturing of CMCs compared to the newly emerging area of additive manufacturing.

matrix (SiC/SiC) materials are a leading CMC for such applications (Refs. 1 to 6). However, the cost of the materials, the complexity in processing, and the limitations in obtaining complex geometries with current CMC fabrication approaches, requires alternative fabrication methods to be investigated such as additive manufacturing (AM).

Additive manufacturing allows custom designed parts to be fabricated layer by layer with much greater complexity into 3D shapes than traditional manufacturing methods. Compared to conventional manufacturing, additive manufacturing of CMCs is in the early stages of development as shown in Figure 1. The efforts in conventional manufacturing of CMCs started over 30 years ago and have continued to progress over the years. The materials are just now reaching maturity and are getting ready to enter service. However, due to high cost of the materials (fibers and coatings) and of the many processing steps (hand layup, fiber coatings, and matrix infiltration), it is not cost effective to conduct small processing runs. Also, with the manual hand layup processes and the use of 2D fiber architectures in cloth form, it is very challenging to obtain large, complex shaped parts for turbine engine components, especially those that require internal channels and 3D geometries. The conventional processing methods tend to restrict the components toward structural rather than multifunctional applications. Additive manufacturing can offer several significant benefits over conventional processing. Prototypes can be rapidly manufactured, small batches can be produced economically, and tooling and molds are not required, since it is a freeform fabrication approach. AM has been demonstrated for metals and polymers and is at higher technology readiness levels (TRL) than for ceramics. While research into the additive manufacturing of ceramics is starting to increase, there has been even less activity reported in the literature for the additive manufacturing of ceramic matrix composites. While there are many additive manufacturing approaches (Refs. 7 and 8), most do not allow the versatility to include fiber reinforcement additions except laminated object manufacturing (LOM) and power bed processing methods.

LOM is a very promising method for fabricating continuous fiber reinforced CMCs that are most similar to current CMCs which have 1D or 2D fiber architectures. In the LOM process, layers of green or adhesive-coated laminates are cut with a laser and then successively stacked and then bonded or glued together to form the part from the bottom to the top. There are only a few references that appear in the literature for the laminated object manufacturing of SiC-based ceramics and fiber reinforced ceramic composites. Windsheimer and Travitzky et al. (Refs. 9 and 10) have demonstrated the fabrication of a nonfiber reinforced material using preforms derived from preceramic paper to obtain a Si-SiC material.

Also, biomorphous SiSiC composites have been fabricated by Weisensel et al. (Ref. 11) by LOM in which pyrolyzed paper sheets and phenolic resin were used to make biocarbon preforms. The biocarbon preforms had a 34 percent reduction in weight after pyrolysis, and the 69.4 percent porous preforms were further densified by a silicon (Si) liquid infiltration step. Upon analysis, it was found that the materials had 16 vol% unreacted carbon and 23 vol% residual silicon that had infiltrated into the porous regions of the laminates. It should be noted that when considering such materials and processes for high temperature and turbine engine applications, the residual silicon is not desirable since it will limit the use temperatures to below 1300 °C.

As far as the LOM of CMC materials, Klosterman et al. (Ref. 12) have reported on the use of bilayer materials that had ceramic grade Nicalon (CG-Nicalon) fiber prepregs stacked in alternating layers with monolithic ceramic tapes. Composite properties suffered due to weak interlayer bonding. Also, low flexural strength was observed due to an insufficient fiber coating and poor high temperature stability of the SiC (CG-Nicalon) fibers. In recent work by the authors (Ref. 13), laminated object manufacturing of SiC/SiC composites was reported. High temperature silicon carbide fiber prepregs were developed and processing parameters were optimized to give the desired SiC/SiC compositions with single step conversion to SiC matrix. Due to the high conversion to SiC, secondary infiltration steps to further densify the composite are not required, and the material will be suitable for use temperatures above 1300 °C, since it does not contain any free silicon.

The other additive manufacturing techniques that are well suited for fabricating CMCs are those methods which use powder bed processing, since micron sized chopped fibers, nano sized fibers, and nanotubes can be easily added to the powder mix. Powder bed processing techniques include selective laser sintering, electron beam sintering, and binder jet 3D printing. These techniques, as with most AM techniques, start with a representation of the part in the form of a computer-aided design (CAD) file which is converted to a stereolithography (STL) file. The STL file represents the part in cut layers which are to be printed as the part is built up. One of the powder bed approaches, binder jet, is illustrated in Figure 2 (Ref. 14). A binder is dispensed from the nozzle of a print head and selectively deposited onto the powder bed surface and coats the powders so that they bond to one another. As each cross-section is complete, the build platform is lowered slightly, and a new layer of powder of a designated thickness is spread over its surface. The process is repeated until the whole part is completed.

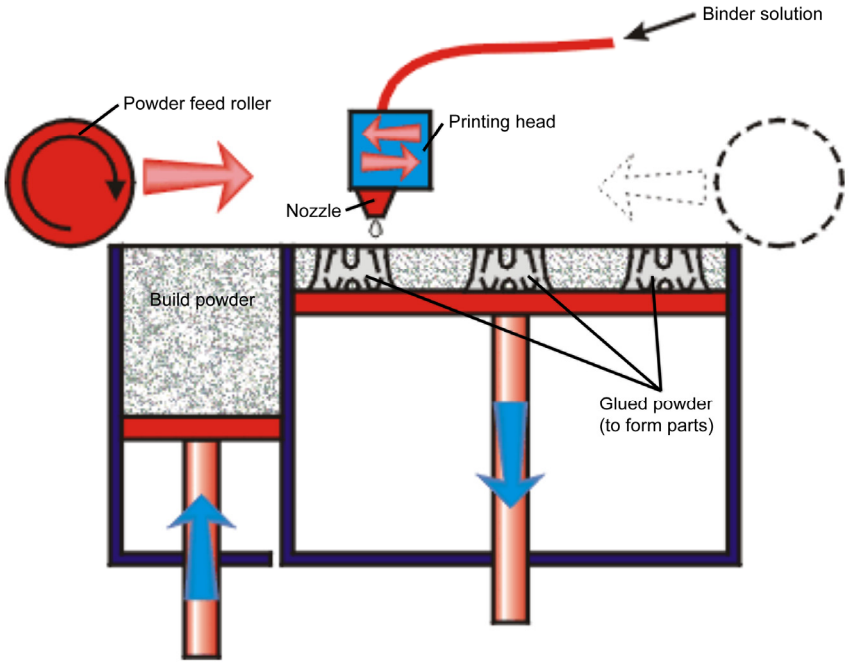

Figure 2.—Illustration of the binder jet additive manufacturing process (Ref. 14).

All three of the powder bed approaches are similar in that the part is formed in a build box filled of loose powder. The main difference is in the way the powders are solidified to form the shape. Selective laser sintering is a thermal method in which a highly focused laser beam is used to densify powders by causing necking between adjacent powders and further consolidation due to volume diffusion and sintering (Ref. 15). Selective laser sintering of SiC powders without binders but with secondary silicon (Si) infiltration has been demonstrated (Ref. 16). Laser micro sintering was used to form micron sized shapes from a blend of Si, SiC, and carbon (C) powders (Ref. 17). Also, a lower temperature process called selective laser curing was demonstrated on a mix of polymethylsilsesquioxane (PMS) preceramic powder mixed with SiC powder (Ref. 18). The porous Si-O-C/SiC material was densified with liquid silicon and turbine wheel shapes were demonstrated. In the electron beam sintering method, the process occurs under a vacuum using a high-energy electron beam as the heat source for melting and fusing powders (Ref. 19). In the binder jet method, instead of a heat based approach, a binder is dispensed from the nozzle of a print head. Schlier et al. demonstrated the 3D binder jet printing of lattice structures of silicon infiltrated silicon carbide for reactors in piston engines (Ref. 20). In our work presented here, we advance the technology beyond the current state of the art by pursuing additively manufactured SiC materials which contain no remaining free silicon and include the addition of SiC fiber reinforcement for higher temperature capability and improved mechanical properties.

The additive manufacturing work reported here is the third part in a series of reports. The corresponding first report in the series provided details on a system study to determine the benefits of replacing metallic turbine engine components with polymer and ceramic matrix composite materials. System benefits were reported for weight reduction and reduced fuel consumption when material replacements were done for critical turbine engine components (Ref. 21). The objective of this work was to develop a processing approach for additively manufacturing ceramic matrix composite materials using the binder jet method. Since there was not a basis within NASA GRC or rp+m, as well as within the wider scientific community, the technology had to be developed from a fundamental level. Different SiC powders with median sizes ranging from 9.3 to 53.0 μm were investigated solely and in bimodal powder blends in order to maximize powder packing. Small SiC fibers were added to the powder bed for the fabrication of ceramic matrix composites. Various infiltration approaches were investigated. Densities were determined for printed coupons. Microstructural analysis was conducted on polished cross-sections using optical and scanning electron microscopes. Mechanical properties of select materials were evaluated in four point bend tests. The additive manufacturing of complex turbine vanes shapes of two sizes was demonstrated using the binder jet 3D printing method.

Experimental Details

To conduct binder jet printing of SiC ceramics and CMCs, a M-Flex print machine by ExOne was used as illustrated in Figure 3. The powder bed was filled with SiC powders to first manufacture unreinforced materials. In the second phase of development, SiC fibers were added to the powder bed powder mix to manufacture fiber reinforced CMCs. The powders that were utilized to fill the powder bed were Carborex SiC grit powders (Washington Mills AS) in grit sizes of F220, F240, F360, and F600. The particle size distributions and composition are shown in Table 1 (Ref. 22). The particle size distribution for F220 was not provided but was added according to the standard of the Federation of the European Producers of Abrasives (FEPA) which is followed by Washington Mills AS. Figure 4 shows the shape and size distribution for the F240 and F360 powders. It can be seen that the powders had a coarse irregular shape rather than a spherical shape. The powders were used singularly and in bimodal powder distributions to investigate particle packing. Fiber additions, ranging from 25 to 75 vol%, were added to the powder mix to manufacture fiber reinforced composite materials. The fiber reinforcement was Si-TUFF SiC fiber (Advanced Composite Materials, LLC). The manufacturer reports fiber dimensions of 7 μm mean diameter by 65 to 70 μm mean length (Fig. 5).

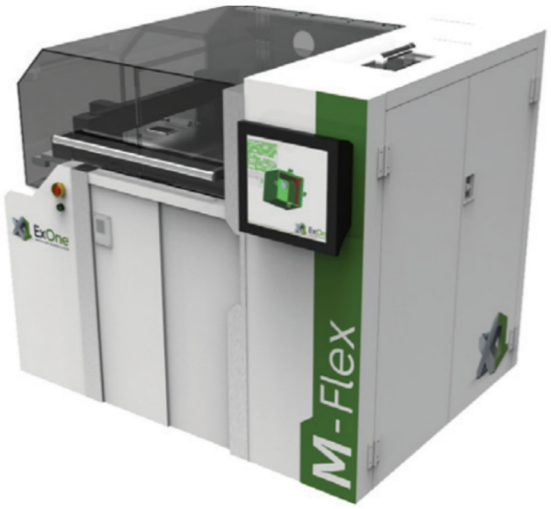

Figure 3.—The ExOne M-Flex print machine.

TABLE 1.—DETAILS OF SIC POWDER USED IN PRESENT WORK SHOWING PARTICLE SIZE DISTRIBUTION AND CHEMICAL ANALYSIS (REF. 22)

Grit designation	dS3-value max. µm	Median grain size dS50-value µm	dS94-value min. µm
F220	75	53.0±3.0	45
F240	70	44.5±2.0	28
F360	40	22.8±1.5	16.5
F600	19	9.3±1.0	3

Particle size distribution measured on Beckman Coulter Multisizer 3, according to FEPA 42-2:2006.

Grit range	% SiC	% Free C	% Si	% SiO_2	% Fe
F240 to F600	99.20	0.15	0.25	0.40	0.07

Chemical analysis (in weight percent) according to FEPA 45-1986, R1993 resp. ISO 9286.

(a) SiC powders (Carborex F240)

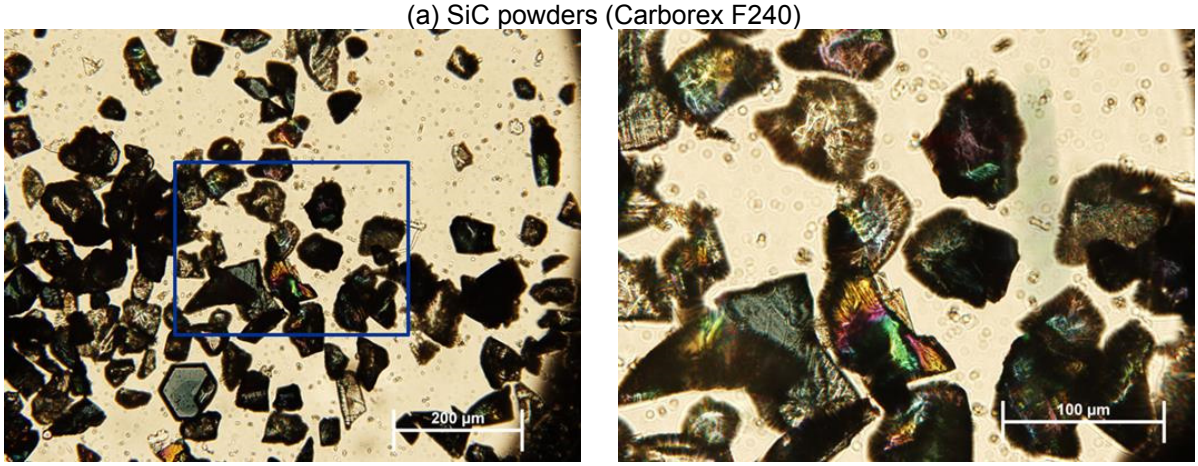

(b) SiC powders (Carborex F360)

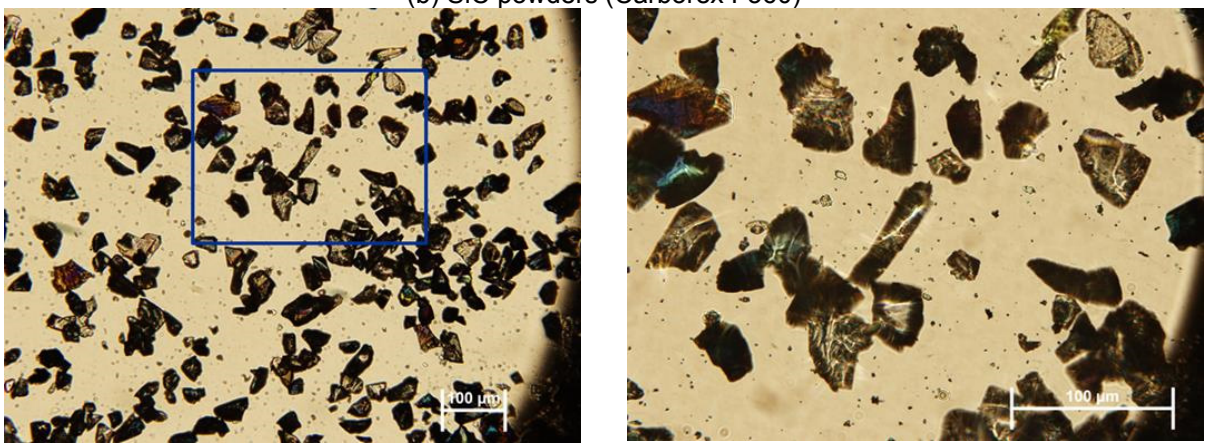

Figure 4.—Optical micrographs at the same magnifications of the SiC F240 (a) and F360 (b) powders on a glass slide.

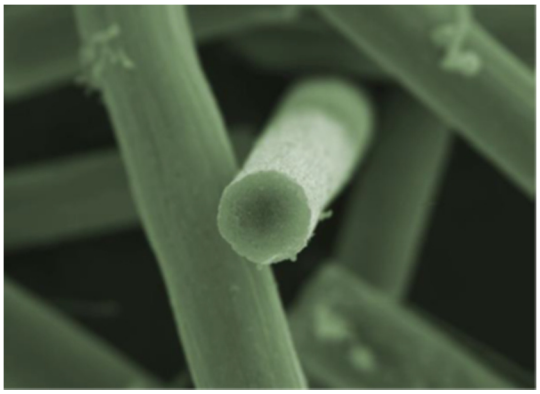

Figure 5.—Si-TUFF SiC fibers (Advanced Composite Materials, LLC).

Two sizes of samples were additively manufactured. The first size was used for microstructural analysis and secondary infiltration trials and had dimensions of approximately 12.7 mm wide by 25.4 mm long by 4.0 mm thick. The second, relatively larger size of coupon, had dimensions of approximately 50.8 by 50.8 by 4.0 mm and was used for mechanical testing. As each layer is built up in the ExOne M-Flex machine, an ExOne binder that is a polymer based ink is used to rigidly link the powders as the green body is formed. Following green body printing, the samples were infiltrated under vacuum with

either a polycarbosilane or a phenolic resin. The polycarbosilane that was used was SMP-10 (Starfire Systems) which is a pre-ceramic polymer with a carbon-silicon backbone that is converted to SiC during pyrolysis. The phenolic resin was loaded with nanoparticles and provided a source of carbon during pyrolysis. Pyrolysis of all printed and infiltrated samples was conducted in a tube furnace under flowing argon with a 30 min. hold at 1000 °C. Other infiltration approaches were investigated for further densifying the coupons. One approach was to load the SMP-10 infiltrant with either 0.7 μm or 0.8 μm average grain size SiC powders and then conduct vacuum infiltration into the green printed coupons. Another approach was to conduct multiple iterations of the polycarbosilane vacuum infiltration and pyrolysis steps. In another approach, pure silicon was melt infiltrated into selected coupons at 1450 °C in vacuum to fill in the porous interior to demonstrate full densification of the coupons. Several print runs were conducted to investigate the various combinations of constituents to include single powder and two powder blends with phenolic infiltrant or SMP-10 infiltrant with and without 0.7 μm and 0.8 μm SiC powder loading, and with and without the addition of reinforcing Si-Tuff SiC fibers added to the powder bed at volume percentages of 25 to 75 vol%.

Microstructural analysis of polished cross-sections of printed samples was conducted using optical and field emission scanning electron microscopes. Selected microscopy will be presented in the results section to illustrate the effects of different constituents and processing steps. Several of the larger samples (50.8 by 50.8 by 4.0 mm) underwent 2 to 3 extra infiltration and pyrolysis cycles where SMP-10 was vacuum infiltrated into the samples to further fill the porous interior and increase the density. These coupons were then surface ground to a flat surface and bend bars were machined with dimensions of 50 mm long by 4 mm wide and roughly 2.5 mm thick. There were variations in thickness among the material sets due to different print runs and powder beds. The bend bars were used to assess mechanical properties of the materials through 4 point bend tests. The binder jet method was used to demonstrate the additive manufacturing of two vane shapes of different sizes.

Results and Discussion

Coupons were printed during several print runs each with variations in the constituents and infiltrants. An example of coupons from one set is shown in Figure 6. Four of the smaller coupons (12.7 mm wide by 25.4 mm long by 4.0 mm thick) and two of the larger coupons (approximately 50.8 by 50.8 by 4.0 mm) were printed during each run. The dimensions and weight of the coupons were measured to determine the bulk density of the coupons in their green state after an infiltration step. The dimensions and weight were taken again after a furnace run to pyrolyze the samples at 1000 °C in flowing argon with a 30 min hold. The average density of the six samples from each set are shown in Table 2. The specific details of each material set (powder sizes, powder blends, infiltrant, and infiltrant loading) will not be divulged due to proprietary issues. However the main point of Table 2 is that the densities of the samples are much lower than the theoretical density of bulk SiC which is ~3.2 g/cc. Only trends will be discussed. Initially binder jet processing with single powders was investigated followed by powder blends. It was observed that the larger F240 SiC powders gave higher densities than the smaller F360 SiC powders. Also the SMP-10 infiltration gave higher densities than the phenolic infiltration. Going to a powder blend of two powder sizes as in set F may have provided a slight improvement in density. Adding 25 vol% of 0.7 μm SiC powders to the SMP-10 infiltrant improved the density as noted in comparing sets F, H, and J with no additions in the infiltrant to G, I, and K which had the addition of the 25 vol% SiC powders of 0.7 μm in diameter. For the CMC materials, sample sets M, N, and O show that as the vol% of SiC fiber increases from 35 to 45 to 65, respectively, the density remains about the same. For sets R to U which were phenolic infiltrated samples, the densities were relatively low. It was noted that after pyrolysis, there was excessive flaking at the surface which was assumed to be an overcoat of the phenolic. Microscopy will be conducted in the future to determine the extent that the phenolic infiltrated the interior of these samples. In order to further densify the samples, optimized processing steps and other processing approaches need to be investigated to include multiple infiltration cycles and melt-infiltration.

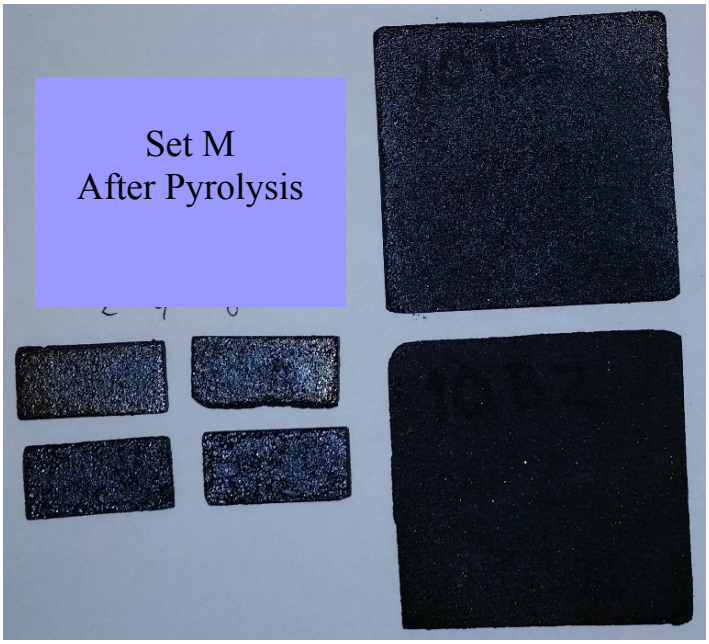

Figure 6.—An example of one of the coupons sets that is printed during a binder jet print run.

TABLE 2.—AVERAGE DENSITIES OF THE SAMPLE SETS IN THEIR GREEN STATE AND AFTER PYROLYSIS

Sample densities (g/cc)		
	Green	Pyrolyzed
Set A	1.60	1.55
Set B	1.54	1.47
Set C	1.21	1.26
Set D	1.01	1.02
Set E	1.54	1.53
Set F	1.71	1.66
Set G	1.95	1.94
Set H	1.68	1.62
Set I	1.78	1.80
Set J	1.57	1.48
Set K	1.73	1.68
Set L	1.47	1.44
Set M	1.65	1.60
Set N	1.51	1.53
Set O	1.53	1.57
Set P	1.50	1.49
Set Q	1.36	1.27
Set R	1.08	0.92
Set S	0.99	0.93
Set T	0.91	0.86
Set U	0.87	0.87

Microstructural analysis of polished cross-sections of a sample from each material set was conducted using optical and scanning electron microscopy. Micrographs from select samples are presented to illustrate the results obtained from using the different constituents and infiltration methods. The cross-section of a sample from Set A is shown in Figure 7. This sample was printed from Carborex F360 SiC powder and had the SMP-10 infiltration. Macro views of the cross-section at the ends and center of the sample are shown in Figure 7(a). It should be noted that the three macro-views represent only about 40 percent of the full length of the cross-section. The two black arrows in-between the three views represents the 60 percent of the cross-section that is not shown. Figure 7(b) shows a higher magnification view of the interior of the sample. Larger pockets of porosity are seen in the macro view while the micro view shows that the individual powders are not tightly packed, and there is minor contact between the SiC powders. The sample underwent one infiltration with SMP-10 followed by pyrolysis. It is seen that the infiltrant does not uniformly coat the powders but rather is a relatively thick deposit on some portions of the powder surfaces. Similar micrographs are shown in Figure 8 which was made from F240 Carborex SiC powders. Main points, compared to Figure 5, are that a gap between printed layers was observed at the right edge of the sample cross-section (Fig. 8(a)), and the powders seem a little more elongated in one-dimension and narrow in the other (Fig. 8(b)).

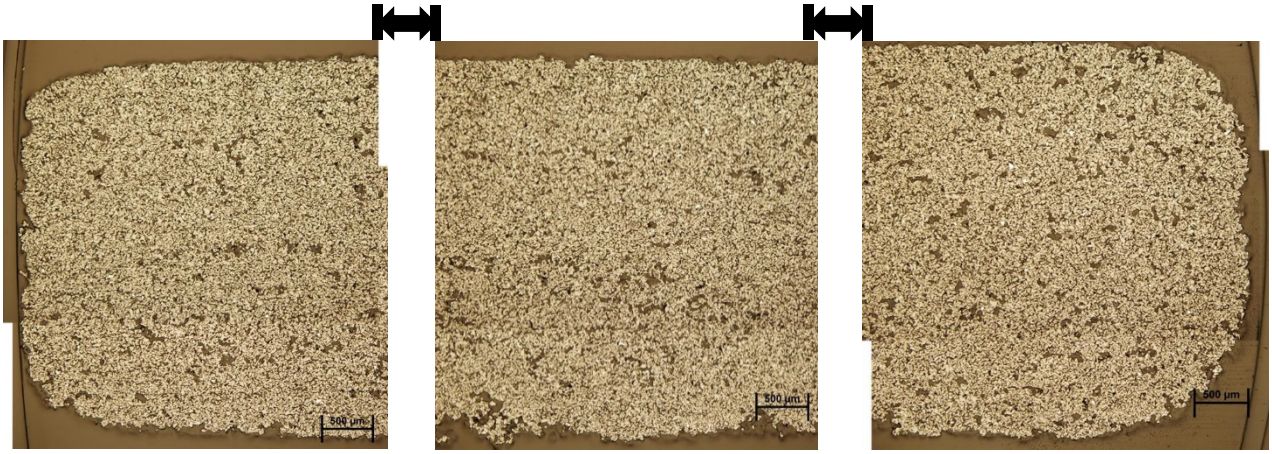

(a)

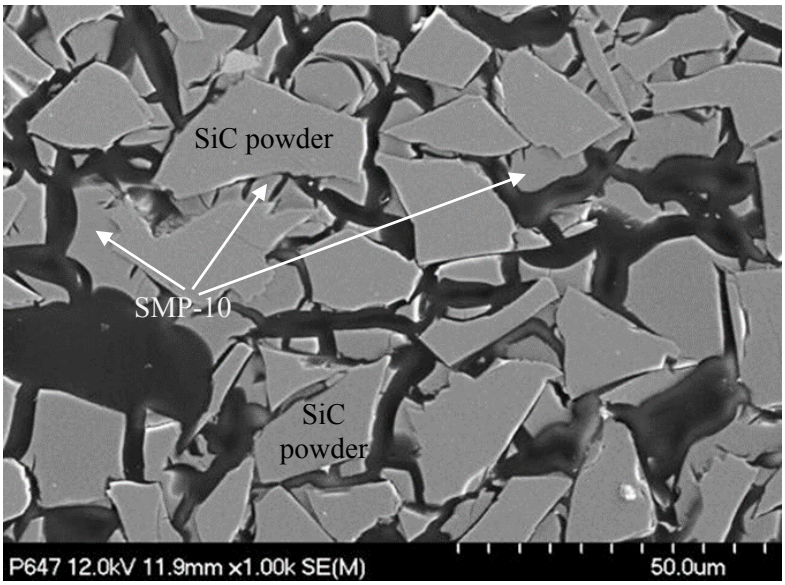

(b)

Figure 7.—Polished cross-section of a sample from Set A: Carborex F240 SiC powders with SMP-10 infiltration. Optical micrographs of sections at the ends and middle of the cross-section (a) and a scanning electron micrograph from the middle of the cross-section (b).

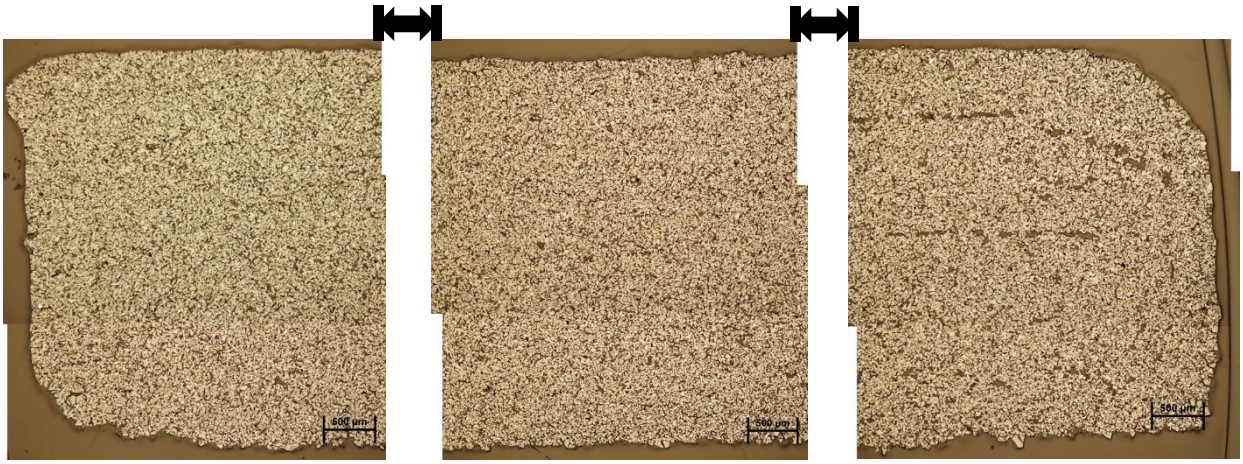

(a)

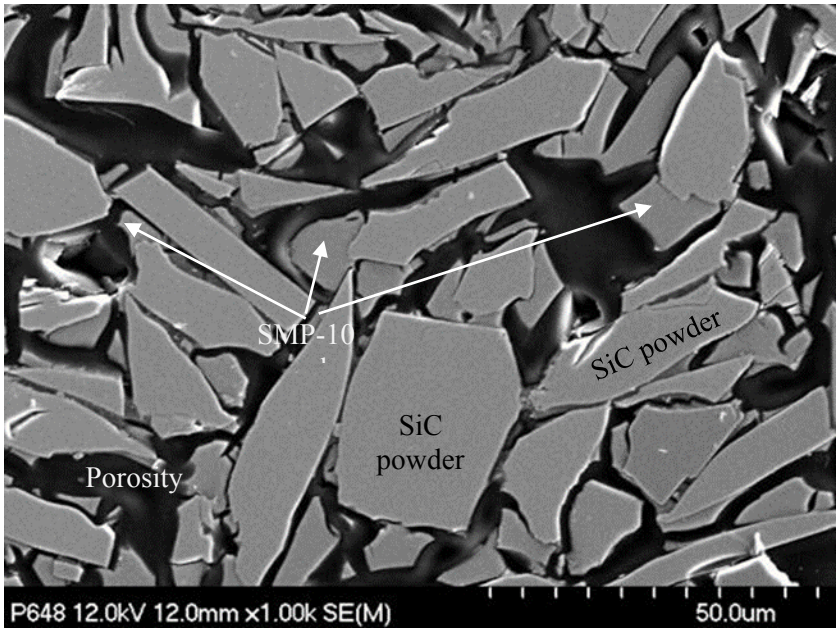

(b)

Figure 8.—Polished cross-section of a sample from Set B: Carborex F360 SiC powders with SMP-10 infiltration. Optical micrographs of sections at the ends and middle of the cross-section (a) and a scanning electron micrograph from the middle of the cross-section (b).

The microstructure of a sample from Set C is shown in Figure 9 which was made from the F240 SiC powder and was infiltrated by the powder loaded phenolic. The SiC powders were not tightly packed and the single infiltrant step only slightly filled in the porosity. The infiltrant was more concentrated at the sample edge but it was also observed further into the interior. The close-up view of a concentrated region of the infiltrant shows detail of its powder loading.

The densest set of samples was Set G, which had an average density of 1.94 g/cc. Figure 10 shows the microstructure of a sample from Set G, which was made from a blend of 90 vol% F240 and 10 vol% F360 Carborex SiC powders. The SMP-10 infiltrant was loaded with 25 vol% 0.7 μm SiC Powder. As seen in the figure on the left, the one infiltration of the loaded SMP-10 gave a much better result in densifying the porous interior and surrounding the F240 SiC powder than compared to the results in Sets A and B which did not have powder loaded SMP-10. The figure on the right shows greater detail of how the 0.7 μm powders and the SMP-10 fill in around and have good contact with the larger Carborex powder.

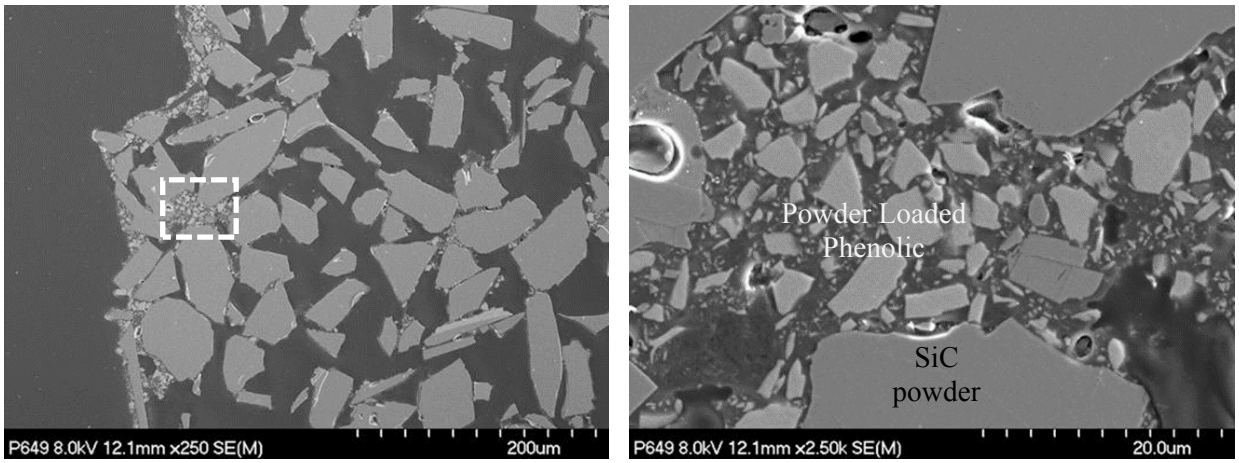

Figure 9.—Polished cross-section of a sample from Set C: Carborex F240 SiC Powders with phenolic infiltration showing scanning electron micrographs at the edge of the sample (left) and a close up view (right).

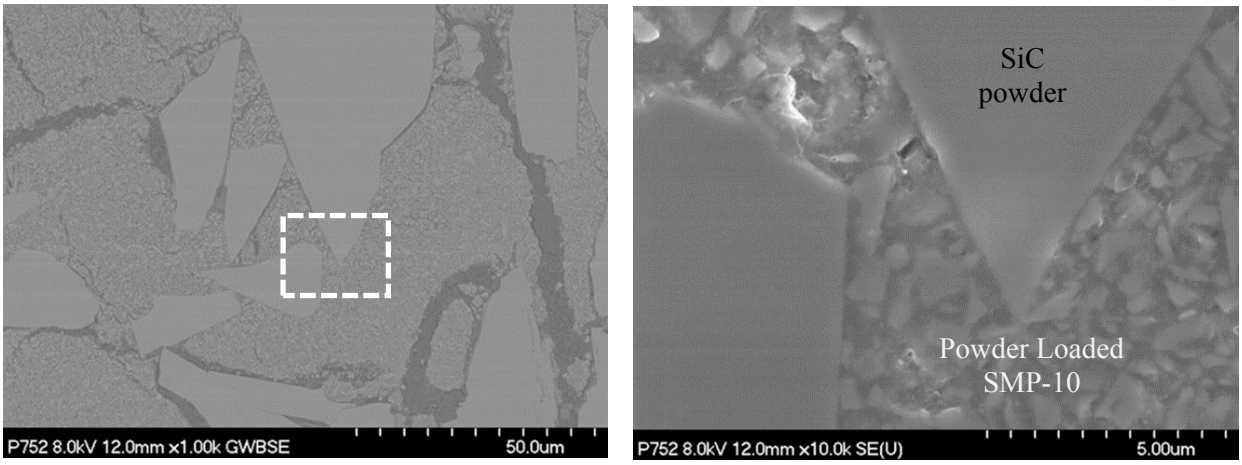

Figure 10.—Polished cross-section of a sample from Set G: 90 vol% F240 and 10 vol% F360 Carborex SiC powder blend with SMP-10 infiltration loaded with 25 vol% of 0.7 μm SiC powder. Scanning electron micrographs of the interior of the sample (left) and a close up view (right).

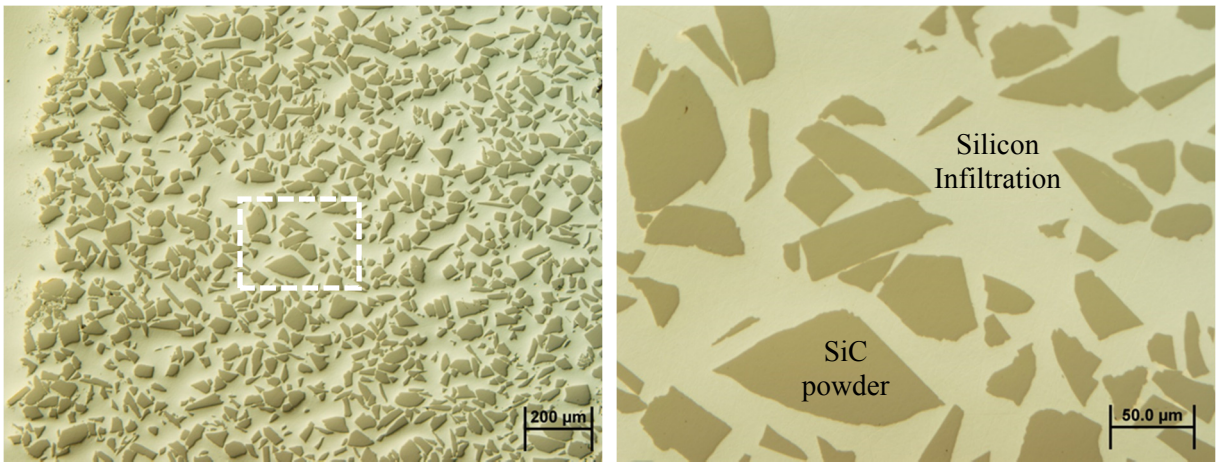

Figure 11.—Polished cross-section of a sample from Set C: Carborex F240 SiC powders with phenolic infiltration followed by a secondary silicon melt infiltration step. Optical micrographs of the edge of the sample (left) and a close up view (right).

In order to demonstrate how well the printed coupons have the potential to be more fully infiltrated and densified, select coupons from the sets underwent a silicon melt infiltration step. Figure 11 shows the cross-section of a sample from Set C that was first infiltrated with phenolic resin and was then infiltrated with liquid silicon during a furnace run in vacuum. As seen in the figure on the left, the silicon completely infiltrated from the edge to the interior. Excess silicon did build up around the exterior of the sample. This effect can be addressed by further optimizing the infiltration step or by doing some post-infiltration machining. The figure on the right shows that the silicon completely surrounded the powders, and no porosity was observed. While good densification results with silicon were observed, the use temperatures of the materials will be restricted to below 1316 °C due to the melt temperature of silicon. Ideally, similar results need to be achieved with the polycarbosilane and phenolic infiltration approaches or melt infiltrations need to be done with higher temperature phases.

Once experience was gained in fabricating only powder loaded materials using the binder jet method, SiC fibers were introduced into the powder bed to begin making fiber reinforced composite materials. Micrographs are shown in Figure 12 of a polished cross-section from Set L which had 65 vol% of a 90 wt% F240 and 10 wt% Carborex F360 SiC Powder mix and 35 vol% of Si-Tuff SiC fiber followed by infiltration by SMP-10. The top micrographs of Figure 12(a) are images from the edge to progressively higher magnifications which shows detail of the Si-Tuff SiC fibers distributed in with the powders. The two bottom images from two additional locations, Figure 12(b), illustrate how the fibers appear in general within the material. The cross sectional views are through the thickness of the sample with the sample being built layer on top of layer in the vertical direction. It can be seen that within the material, the fibers are well distributed with non-preferred orientations. On the horizontal plane fibers are in both the 0° and 90° directions. While it will be difficult to print materials with fibers fully upright, fibers at as much as 45° from horizontal are observed in the vertical plane. The good distribution of fibers in different orientations is expected to contribute to beneficial composite properties for the material.

In order to further densify the materials, extra infiltration steps were conducted for 50.8 by 50.8 mm panels from several of the materials sets. Beyond the infiltration as indicated in Table 2, additional iterations of SMP-10 vacuum infiltration followed by pyrolysis in a furnace were conducted. Figure 13(c) shows the starting density and the density of the panel after the 2 to 3 additional infiltration iterations. The extra infiltrations increased the densities by 0.20 to 0.55 g/cc. Most of the increase in density occurred in the first two infiltrations with less effect from the third infiltration. An example of a panel that has been further densified and bend bars that were machined from the panel are shown in Figure 13(a) and (b).

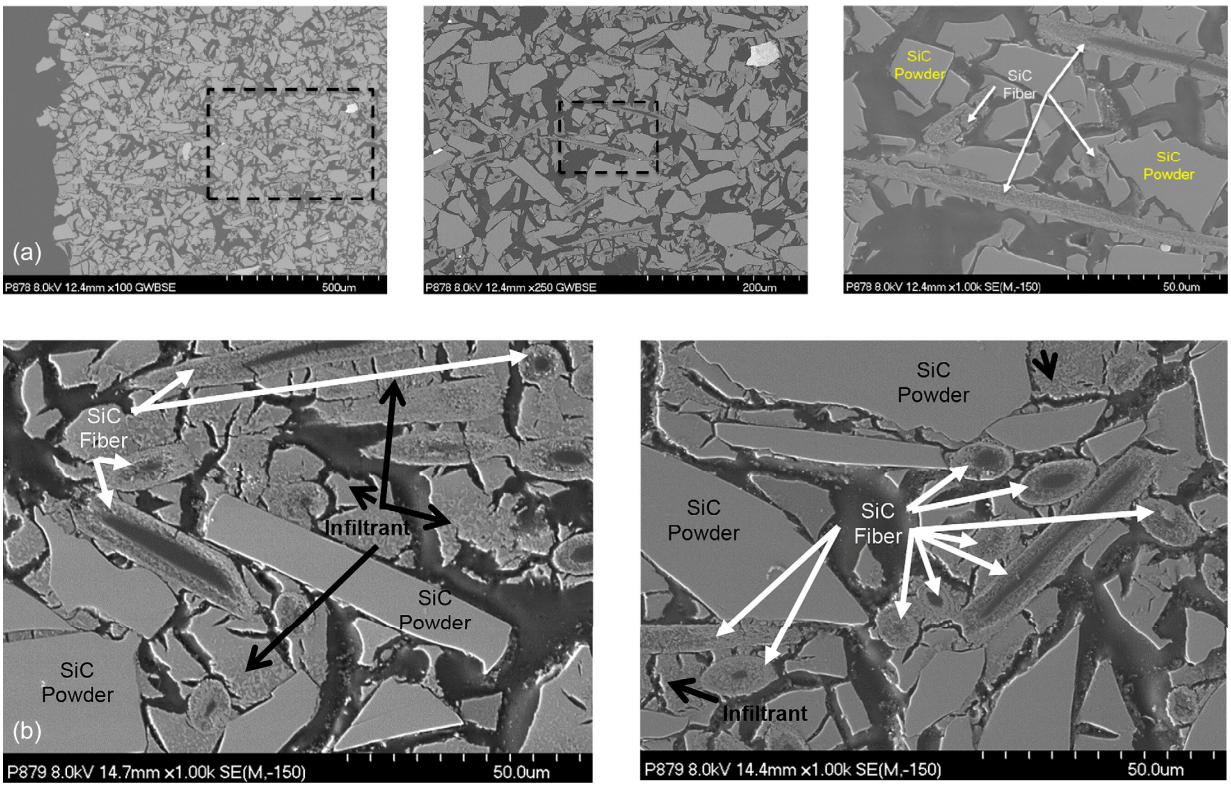

Figure 12.—Polished cross-section of a sample from Set L: 65 vol% of 90 wt% F240 and 10 wt% Carborex F360 SiC Powder mix and 35 vol% of Si-Tuff SiC fiber with an infiltration of SMP-10. Scanning electron micrographs of the edge of the sample and a close up view are shown (a) with additional views at other locations showing detail of the Si-Tuff SiC fibers (b).

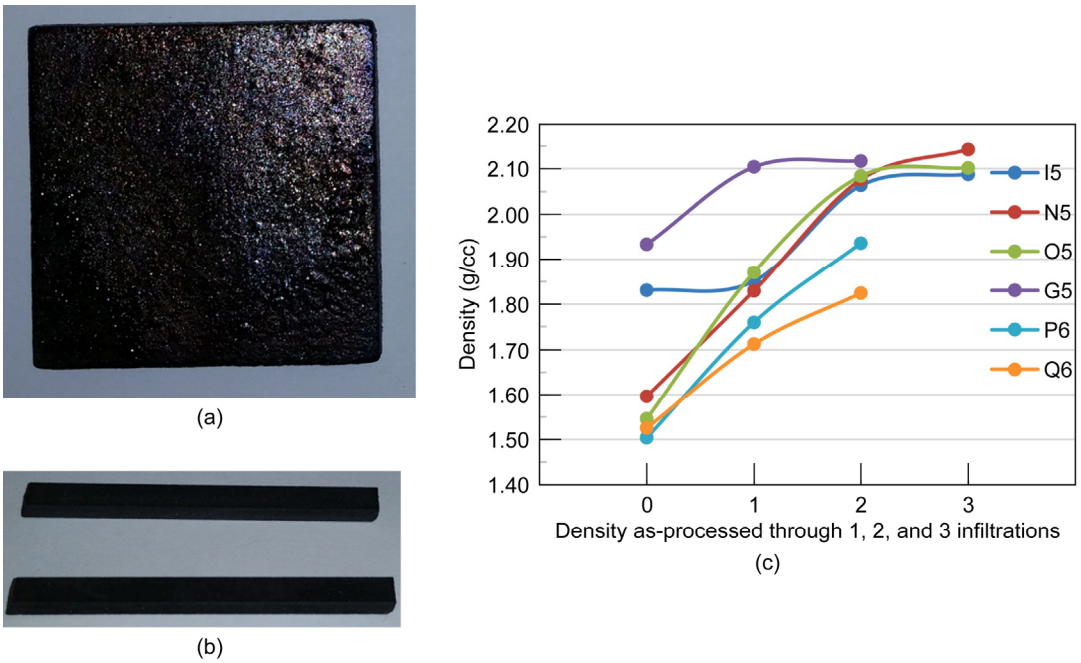

Figure 13.—An example of a 50.8 by 50.8 mm panel that had undergone extra infiltrations (a) and bend bars that had been machined from the panel which had been surface ground (b). The improvements in panel densities with infiltration iterations is shown where the legend correlates to the material set and the print run sample number (c).

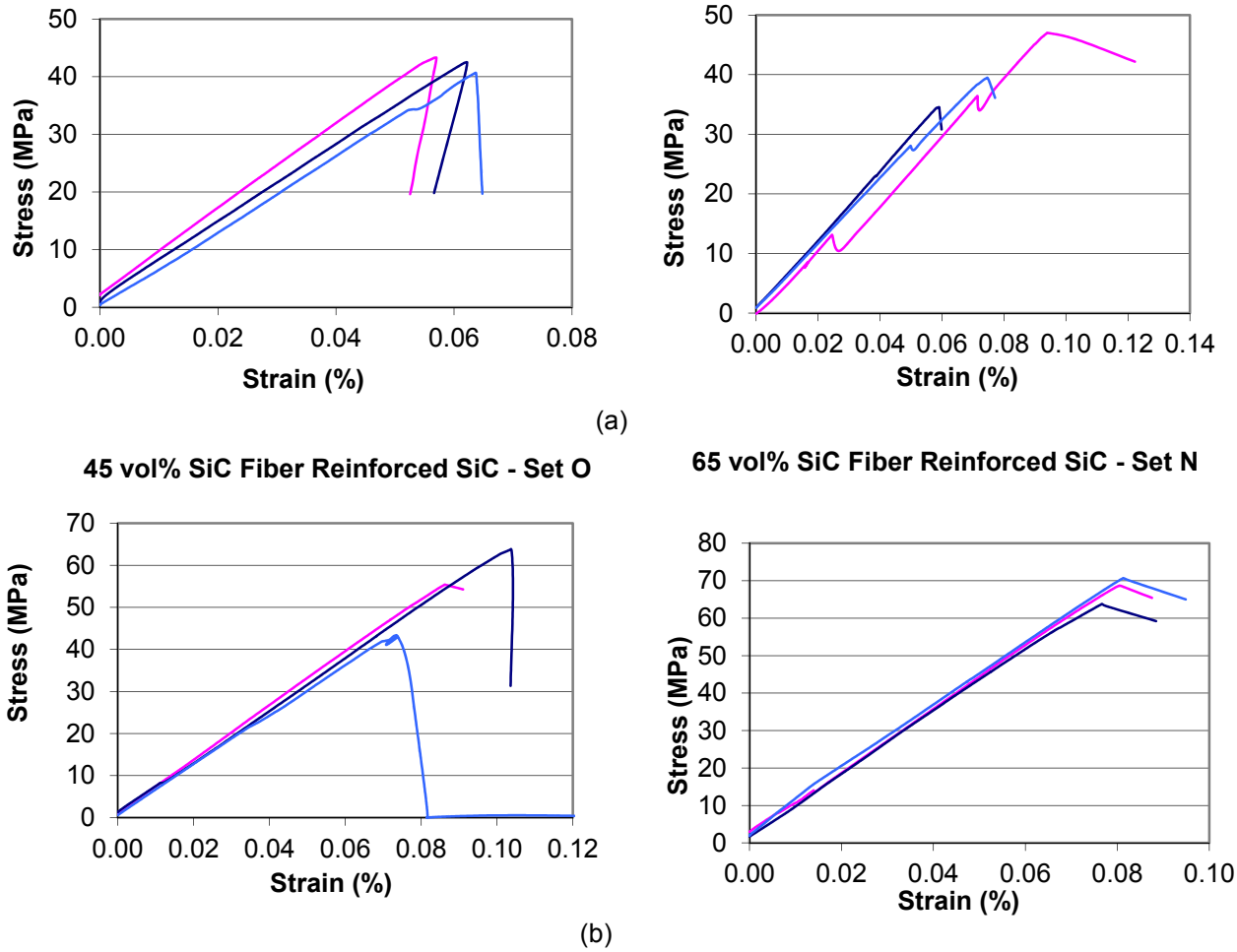

Figure 14.—Plots of stress versus strain for the results of three bend bar tests from each panel for the nonreinforced materials (a) and the Si-Tuff SiC fiber reinforced materials (b).

The results from four point bend tests are given in Figure 14 for two nonreinforced panels, Sets I and G, and two fiber reinforced panels, Sets N and O. Three bend bars from each panel were tested at room temperature. Overall, the fiber reinforced ceramic matrix composite materials had much higher strengths and strains to failure compared to the non-fiber reinforced materials. One bend bar from Set I had a relatively high strength and strain to failure which was comparable with results of the reinforced materials. The highest strains to failure were from Set O which had 45 vol% fiber loading. The highest strengths to failure were from Set N which had 65 vol% fiber loading.

Fractography was conducted on tested samples to observe for composite behavior. The bend tests showed improvements in the stress and strain to failure for fiber reinforcements. However, composite behavior would more truly be demonstrated from the presence of fiber pullout from fracture surfaces. Figure 15 shows the fracture surface of a bend bar from Set N. The material does appear dense due to the three extra infiltration steps. Fiber pullout was not observed. Instead areas of fibers bridging porous regions were observed (Fig. 15(a) and (c)). Only in rare cases was fiber pullout observed (Fig. 15(b)). It should be noted that the fibers were uncoated. In ceramic matrix composite materials, the observance of composite properties is dependent on an interfacial fiber coating. For the materials presented here, the fibers are rigidly bonded to the matrix due to the absence of an interphase. This can cause the material to behave more like a monolithic material with the fibers providing little benefit. In future work, fiber coatings will be investigated for improving the composite behavior of the material.

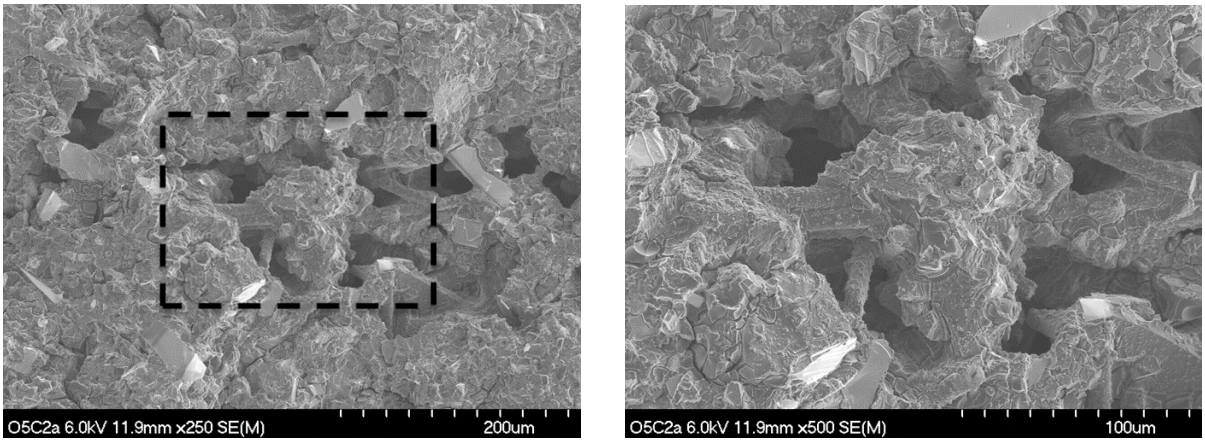

(a) Location 1

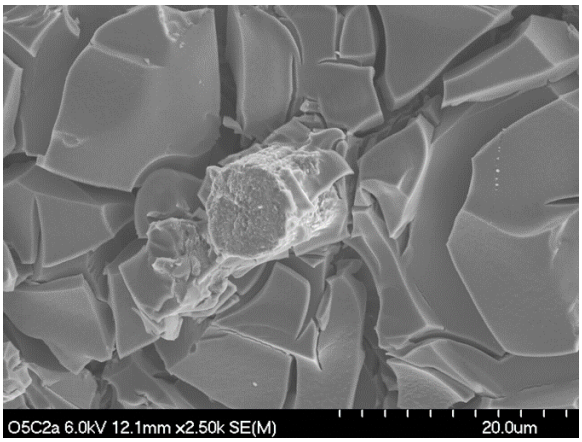

(b) Location 2

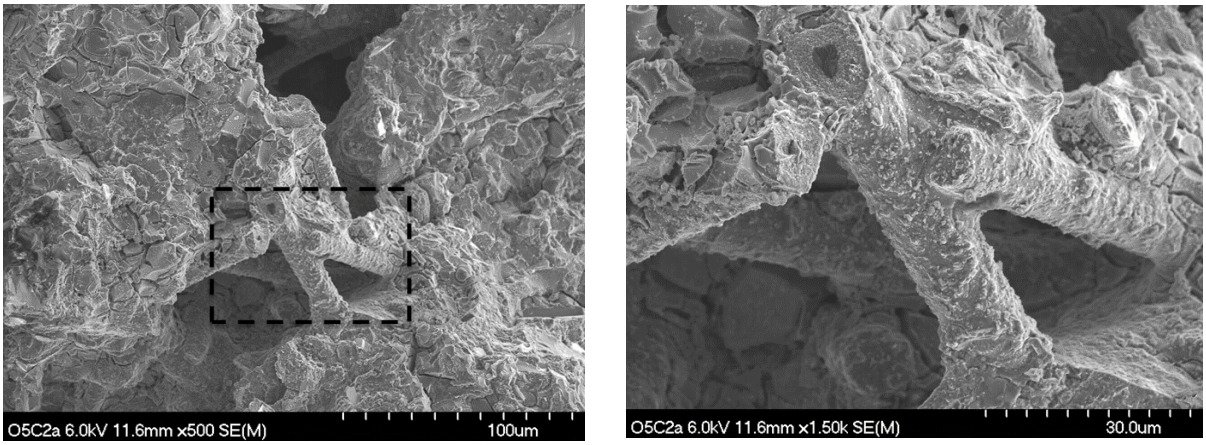

(c) Location 3

Figure 15.—FE SEM of a fracture surface at three locations for a sample from Set N with 65 vol% SiC fiber.

(a) (b)

Figure 16.—Demonstration of the additive manufacturing of turbine engine CMC components (20 vol% SiC fiber). Two smaller first stage nozzle segments in addition to two high pressure turbine nozzle segments for a cooled doublet vane (a). Aligned cooled double vane sections (b).

The ability for the binder jet method to be used to fabricate relevant shapes for turbine engine component applications was demonstrated. Two different sizes of turbine vanes were printed to include larger size high pressure turbine nozzle segments for a cooled doublet vane and two smaller first stage nozzle segments (Fig. 16(a)). Two cooled double vane sections were aligned to illustrate how the sections are placed to form a vane ring section (Fig. 16(b)). While the material processing may need further optimization to improve the properties, it is encouraging that such complex and relevant shapes can be made.

Conclusions

Binder jet 3D printing was used to fabricate ceramic matrix composite materials. Silicon carbide powders of different sizes and blends were used in the powder bed to investigate the printability during the printing process such as powder spreading and layer build up and the print quality that resulted by conducting microscopy to look at powder packing, porosity, and infiltration. Single infiltrations of SMP-10 and phenolic only slightly filled in the interior. When the SMP-10 was loaded with sub-micron sized SiC powders, the infiltrant gave a much better result of filling in the interior. Silicon carbide fibers were added to the powder bed to make ceramic matrix composite materials. Microscopy showed that the fibers were well distributed with no preferred orientation on the horizontal plane, and fibers in the vertical plane were at angles as much as 45°. Secondary infiltration steps were necessary to further densify the material. Two to three extra infiltration steps of SMP-10 increased the density by 0.20 to 0.55 g/cc. However, the highest densities achieved were 2.10 to 2.15 g/cc. This is still much lower than the density of fully dense monolithic SiC (~3.00 to 3.20 g/cc) depending on the manufacturing process used for these materials.

Mechanical testing results show that two CMC panels had higher strengths and strains to failure that the samples from the two non-fiber reinforced panels. The highest strengths were from Set N with 65 vol% fiber loading which had an average strength of 66 MPa. Analysis of the fracture surfaces did not reveal pullout of the reinforcing fibers. Blunt fiber failure suggested that there was not composite behavior. The binder jet additive manufacturing method was used to demonstrate the fabrication of turbine engine vane components of two different designs and sizes. The binder jet method has benefits over the conventional manufacturing of CMCs in that prototype and production parts can be fabricated quickly and economically with no tooling and extensive hand layup. Future work will focus on improving the density of the materials by optimizing the powder packing and infiltration. Fiber coatings will need to be investigated.

References

1. F. Christin, "Design, Fabrication, and Application of Thermostructural Composites (TSC) like C/C, C/SiC, and SiC/SiC Composites," Adv. Eng. Mater., (2002) 4: 903–912.
2. J.A. DiCarlo, H-M. Yun, G.N. Morscher, and R.T. Bhatt. "SiC/SiC composites for 1200 C and above," In Handbook of Ceramic Composites, pp. 77–98. Springer US, 2005.
3. M.C. Halbig, M.H. Jaskowiak, J.D. Kiser, and D. Zhu. "Evaluation of ceramic matrix composite technology for aircraft turbine engine applications," In 51st AIAA Aerospace Sciences Meeting including the New Horizons Forum and Aerospace Exposition, pp. 07–10. 2013.
4. R. Naslain, "Design, Preparation and Properties of Non-oxide CMCs for Application in Engines and Nuclear Reactors: An Overview," Composites Science and Technology, Vol. 64, 2 (2004) 155–170.
5. M. Singh and S.R. Levine, "Low Cost Fabrication of Silicon Carbide Based Ceramics and Fiber Reinforced Composites," NASA-TM 107001 (1994), Glenn Research Center, Cleveland, OH.
6. H. Ohnabe, S. Masaki, M. Onozuka, K. Miyahara, and T. Sasa. "Potential application of ceramic matrix composites to aero-engine components," Composites Part A: Applied Science and Manufacturing 30, no. 4 (1999): 489-496.
7. X. Tian, D. Li, and J.G. Heinrich, "Net-Shaping of Ceramic Components by Using Rapid Prototyping Technologies," INTECH Open Access Publisher, 2011.
8. K.V. Wong and A. Hernandez, "A Review of Additive Manufacturing," International Scholarly Research Network, ISRN Mechanical Engineering, Volume 2012, Article ID 208760, 10 pages.
9. H. Windsheimer, N. Travitzky, A. Hofenauer, and P. Greil, "Laminated Object Manufacturing of Preceramic-Paper-Derived Si-SiC Composites," Advanced Materials, 19 (2007) 4515–4519.
10. N. Travitzky, H. Windsheimer, T. Fey, P. Greil, "Preceramic Paper-Derived Ceramics," J. Am. Ceram. Soc., 91, 11 (2008) 3477–3492.
11. L. Weisensel, N. Travitzky, H. Sieber and P. Greil, "Laminated Object Manufacturing (LOM) of Si-SiC Composites," Advanced Engineering Materials, Vol. 6, 11 (2004) 899–903.
12. D. Klosterman, R. Chartoff, G. Graves, N. Osborne and B. Priore, "Interfacial Characteristics of Composites Fabricated by Laminated Object Manufacturing," Composites, Part A, 29 A (1998) 1165–1174.
13. M. Singh, M.C. Halbig, and S.X. Zhu, "Characterization of Matrix Materials for Additive Manufacturing of Silicon Carbide-Based Composites," Advanced Processing and Manufacturing Technologies for Nanostructured and Multifunctional Materials: CESP Volume 35 6 (2015): 41.
14. http://www.uni.edu/~rao/rt/major_tech.htm
15. J-P Kruth, P. Mercelis, J. Van Vaerenbergh, L. Froyen, and M. Rombouts. "Binding mechanisms in selective laser sintering and selective laser melting," Rapid prototyping journal 11, no. 1 (2005): 26–36.
16. W. Löschau, R. Lenk, S. Scharek, M. Teichgraber, S. Nowotny, and C. Richter. "Prototyping of complex-shaped parts and tools of Si/SiC-ceramics by selective laser sintering," Advances in science and technology (1999): B567-B573.
17. A. Streek, P. Regenfuß, F. Ullmann, L. Hartwig, R. Ebert, H. Exner, "Processing of silicon carbide by laser micro sintering," The Proceedings of the 17th Annual SFF Symposium. Vol. 349, 2006.
18. T. Friedel, N. Travitzky, F. Niebling, M. Scheffler, and P. Greil. "Fabrication of polymer derived ceramic parts by selective laser curing," Journal of the European Ceramic Society 25, no. 2 (2005): 193–197.
19. Xibing Gong, Ted Anderson, and Kevin Chou. "Review on powder-based electron beam additive manufacturing technology," In ASME/ISCIE 2012 International Symposium on Flexible Automation, pp. 507-515. American Society of Mechanical Engineers, 2012.

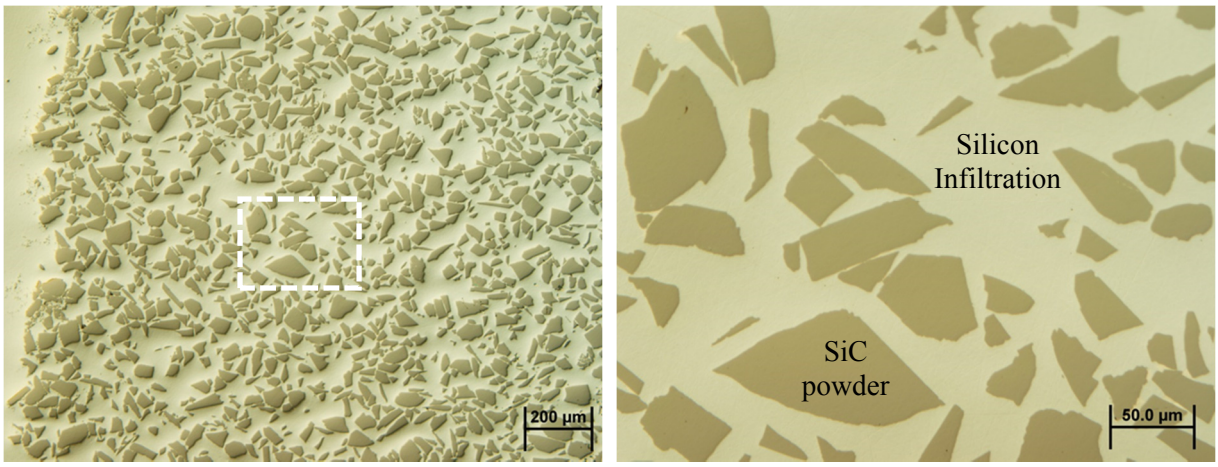

Figure 11.—Polished cross-section of a sample from Set C: Carborex F240 SiC powders with phenolic infiltration followed by a secondary silicon melt infiltration step. Optical micrographs of the edge of the sample (left) and a close up view (right).

In order to demonstrate how well the printed coupons have the potential to be more fully infiltrated and densified, select coupons from the sets underwent a silicon melt infiltration step. Figure 11 shows the cross-section of a sample from Set C that was first infiltrated with phenolic resin and was then infiltrated with liquid silicon during a furnace run in vacuum. As seen in the figure on the left, the silicon completely infiltrated from the edge to the interior. Excess silicon did build up around the exterior of the sample. This effect can be addressed by further optimizing the infiltration step or by doing some post-infiltration machining. The figure on the right shows that the silicon completely surrounded the powders, and no porosity was observed. While good densification results with silicon were observed, the use temperatures of the materials will be restricted to below 1316 °C due to the melt temperature of silicon. Ideally, similar results need to be achieved with the polycarbosilane and phenolic infiltration approaches or melt infiltrations need to be done with higher temperature phases.

Once experience was gained in fabricating only powder loaded materials using the binder jet method, SiC fibers were introduced into the powder bed to begin making fiber reinforced composite materials. Micrographs are shown in Figure 12 of a polished cross-section from Set L which had 65 vol% of a 90 wt% F240 and 10 wt% Carborex F360 SiC Powder mix and 35 vol% of Si-Tuff SiC fiber followed by infiltration by SMP-10. The top micrographs of Figure 12(a) are images from the edge to progressively higher magnifications which shows detail of the Si-Tuff SiC fibers distributed in with the powders. The two bottom images from two additional locations, Figure 12(b), illustrate how the fibers appear in general within the material. The cross sectional views are through the thickness of the sample with the sample being built layer on top of layer in the vertical direction. It can be seen that within the material, the fibers are well distributed with non-preferred orientations. On the horizontal plane fibers are in both the 0° and 90° directions. While it will be difficult to print materials with fibers fully upright, fibers at as much as 45° from horizontal are observed in the vertical plane. The good distribution of fibers in different orientations is expected to contribute to beneficial composite properties for the material.

In order to further densify the materials, extra infiltration steps were conducted for 50.8 by 50.8 mm panels from several of the materials sets. Beyond the infiltration as indicated in Table 2, additional iterations of SMP-10 vacuum infiltration followed by pyrolysis in a furnace were conducted. Figure 13(c) shows the starting density and the density of the panel after the 2 to 3 additional infiltration iterations. The extra infiltrations increased the densities by 0.20 to 0.55 g/cc. Most of the increase in density occurred in the first two infiltrations with less effect from the third infiltration. An example of a panel that has been further densified and bend bars that were machined from the panel are shown in Figure 13(a) and (b).